Tellus SERIES A DYNAMIC METEOROLOGY AND OCEANOGRAPHY
PUBLISHED BY THE INTERNATIONAL METEOROLOGICAL INSTITUTE IN STOCKHOLM

Tellus (2011), 63A, 763–781
Printed in Singapore. All rights reserved

TELLUS

Evaluation of daily temperatures in Central Europe and their links to large-scale circulation in an ensemble of regional climate models

By EVA PLAVCOVÁ [1,2]* and JAN KYSELÝ [1], [1]*Institute of Atmospheric Physics AS CR, Prague, Czech Republic;* [2]*Faculty of Mathematics and Physics, Charles University, Prague, Czech Republic*

(Manuscript received 25 August 2010; in final form 27 December 2010)

ABSTRACT

Reproduction of daily maximum and minimum temperatures, including tails of their distributions and links to large-scale circulation, is evaluated in an ensemble of high-resolution regional climate model (RCM) simulations over the Czech Republic. RCM data for recent climate (1961–1990) are validated against observed data gridded from a high-density station network. We find large biases in mean monthly temperatures and in seasonal extremes, which are significant in most RCMs throughout the year. The results suggest that an RCM's formulation plays a much more important role in summer, whereas in winter RCM performance is closely linked to the driving GCM. Biases are usually larger for extremes than central parts of temperature distributions, and RCMs tend to underestimate the severity of extremes in both seasons. Substantial underestimation of diurnal temperature range throughout the year in all RCMs and a shift of maximum in its annual cycle suggest general errors in simulating climate processes affecting the difference between daytime and nighttime temperatures. Some features of the temperature biases in RCMs are related to deficiencies in the simulation of atmospheric circulation, particularly too strong advection and overestimation of westerly flow at the expense of easterly flow in most RCMs. The general biases in simulating anticyclonic, cyclonic and straight flow also contribute to the underestimated diurnal temperature range.

1. Introduction

The most widely used tools for simulating scenarios of climate change at regional and local scales are regional climate models (RCMs) nested in global climate models (GCMs). Since RCM control outputs, usually evaluated for 1961–1990, suffer from many deficiencies in the reproduction of observed climate conditions, it is necessary to identify sources of these errors and address the deficiencies in further developing the models. A number of papers dealing with validation of control RCM outputs have demonstrated biases in surface air temperatures (over Europe e.g. Jacob et al., 2007; Lenderink et al., 2007; Christensen et al., 2008; Kjellström et al., 2011). It is often reported that the model errors are typically larger in tails of distributions (Kjellström et al., 2007; Kyselý et al., 2008), which are particularly relevant for impacts on ecosystems as well as society. The summary of advances in regional climate modelling within the ENSEMBLES project (http://ensembles-eu.metoffice.com/) are given in van der Linden and Mitchell (2009), section 5: formulation of very-high-resolution RCM ensembles for Europe.

Since one of the key determinants of climate in Europe is the large-scale atmospheric circulation, the temperature biases may depend on the ability of RCMs to capture the circulation regimes and types (e.g. Sanchez-Gomez et al., 2009) and the links between circulation and surface temperature (Turnpenny et al., 2002; Blenkinsop et al., 2009). Kjellström et al. (2011) found that temperature biases in RCA simulations are to a large degree related to errors in how the driving GCMs simulate the large-scale circulation. So, if basic features of the links between circulation patterns and surface temperatures are captured by the RCMs, the temperature biases may be related to errors in the atmospheric circulation rather than in the links between circulation and temperature.

This paper focuses on evaluating recent climate (1961–1990) simulations of surface temperatures over the Czech Republic (Central Europe) and their links to large-scale circulation in an ensemble of high-resolution RCMs. Within the ENSEMBLES project, many RCM integrations over Europe with spatial resolution of around 25 km were made available. The study examines combinations of runs that allow for investigating sources of temperature biases by comparing the same driving GCM in

*Corresponding author.
e-mail: plavcova@ufa.cas.cz
DOI: 10.1111/j.1600-0870.2011.00514.x

Table 1. Summary of the RCMs examined in this study and their acronyms

Institution	RCM	Driving GCM	Reference	Acronym
DMI (Danish Meteorological Institute)	HIRHAM	ECHAM5	Christensen et al. (1996)	hir_ec3
KNMI (Royal Netherlands Meteorological Institute)	RACMO	ECHAM5	Lenderink et al. (2003)	rac_ec3
ICTP (Abdus Salam International Centre for Theoretical Physics)	RegCM	ECHAM5	Giorgi et al. (2004)	rem_ec3
MPI (Max-Planck Institute)	REMO	ECHAM5	Jacob (2001)	reo_ec3
SMHI (Swedish Meteorological and Hydrological Institute)	RCA	ECHAM5	Kjellström et al. (2005), Samuelsson et al. (2011)	rca_ec3
		BCM		rca_bcm
		HadCM3Q3		rca_hd3
		ERA-40		rca_ERA

combination with five different RCMs, and a single RCM in combination with three driving GCMs and the ERA-40 re-analysis (Uppala et al., 2005). The skill of the RCMs in simulating atmospheric circulation, represented by classification derived from circulation indices (Barry and Carleton, 2001), is also evaluated and discussed with respect to temperature errors.

The paper is structured as follows: the data and methods used are described in Section 2, while analysis of models' performance for various temperature characteristics and atmospheric circulation is presented in Section 3. Links between biases in surface temperature and atmospheric circulation are examined in Section 4. Discussion and conclusions follow in Sections 5 and 6.

2. Data and methods

2.1. Regional climate models (RCMs)

The RCM output examined in this study was obtained from the RT3 database of the EU-FP6 ENSEMBLES project (http://ensemblesrt3.dmi.dk/). The list of models and their acronyms is given in Table 1. The RCM simulations corresponding to the control period of 1961–1990 are split into two parts: we investigate control simulations of five RCMs driven by the same GCM (ECHAM5; Roeckner et al., 2006) and, separately, four runs of the RCA model (Kjellström et al., 2005) driven by three different GCMs (ECHAM5, BCM, and HadCM3) and the ERA-40 re-analysis (Uppala et al., 2005). This allows for examining differences between model simulations due to the choices of RCM and driving GCM. All models have a spatial resolution of about 25 km (0.22°), and they use the same grid except for RegCM.

2.2. Gridded observed data (GriSt)

Since each RCM grid box value is a best estimate average of the grid square, the model data and point observations (stations) cannot be compared directly. In this study, RCM daily maximum and minimum air temperatures (Tmax and Tmin) are evaluated against gridded daily data (GriSt) interpolated from a high-density station network operated by the Czech Hydrometeorological Institute. The observations were gridded onto the same 0.22° rotated pole grid that is common to all RCMs except for RegCM. The altitude of the grid boxes was taken from the high-resolution European gridded data set (E-OBS, Haylock et al., 2008) and closely corresponds to orography in most of the RCMs examined. We used the GriSt data set to represent observations since a previous study showed that the E-OBS data are biased over the Czech Republic, particularly for Tmin and in tails of temperature distributions (Kyselý and Plavcová, 2010). The GriSt data set is superior due to a much denser station network providing input data (268 stations with daily temperature measurements formed the input data set in GriSt, while only 13 stations were available in this area for E-OBS), and consequently, much smaller search radius (which does not lead to oversmoothing of data) may be applied in the interpolation.

The interpolation method was introduced by Kyselý et al. (2008), who evaluated temperature extremes in control simulations of RCMs from the PRUDENCE project, and it is described in detail in Kyselý and Plavcová (2010). The quality control and homogenization using the methodology described in Štěpánek et al. (2009) were applied to the input station data. The grid point series of Tmax and Tmin were calculated by the inverse distance weighting method (e.g. Isaaks and Srivastava, 1989) using data from all stations within a distance of 20 km from a given grid point; if the number of stations within the radius was smaller than 6, more distant stations were added until the condition of at least six stations for the interpolation was met. Before applying inverse distance weighting, the data at neighbouring stations were standardized with respect to the grid point altitude using a linear regression based on altitudes and daily temperatures for each calendar month individually. For the weighted average using the inverse distances, the power of 0.5 (square root) was found suitable as it characterizes an 'areal average' for a grid point better than do higher powers. Since the input data set is

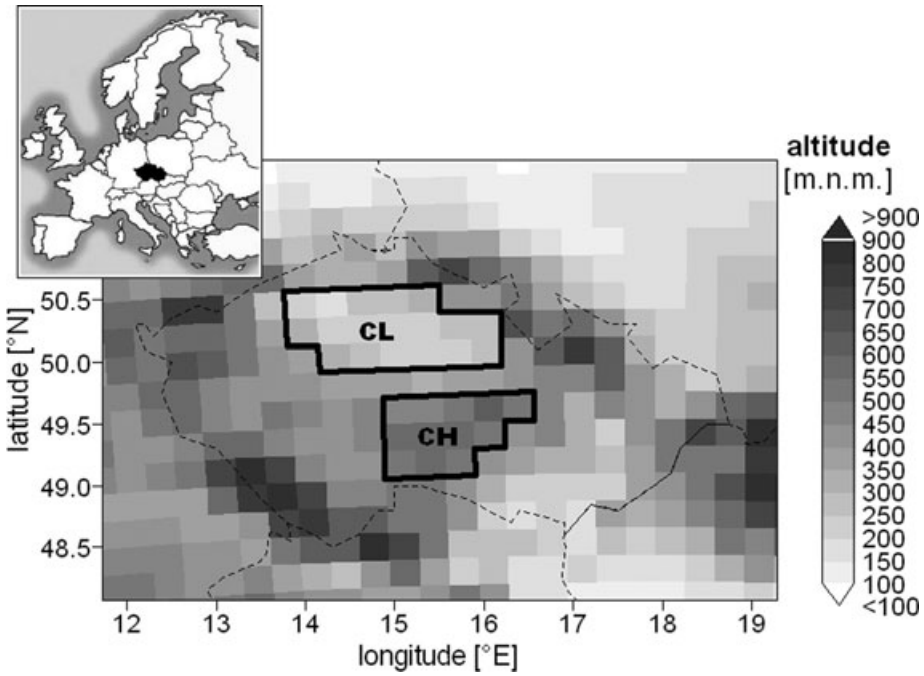

Fig. 1. Regions under study (Central Lowland, CL; Central Highland, CH). Altitudes of grid boxes correspond to the observed data set (GriSt).

a high-density one, the GriSt data are constructed so that the grid box values are relatively 'local' (the search radius is small, particularly compared to E-OBS) but represent 'areal averages' rather than point values.

The GriSt data set is evaluated in detail (against the E-OBS gridded data set and station averages) in Kyselý and Plavcová (2010).

2.3. Method

For the evaluation of the RCMs, two specific regions in the Czech Republic were defined with respect to the basic grids used in the RCMs and the gridded observed data set: Central Lowland (CL) and Central Highland (CH) regions (Fig. 1). While the CL region represents a lowland area (one of two main agricultural regions in the Czech Republic), with average altitude of grid boxes at 257 m a.s.l., the CH region is a highland area with mean altitude of 549 m a.s.l. (both values refer to the gridded observed data set). The two regions differ in many climatological characteristics, see for example, Kyselý (2010). Mean series of daily *T*max and *T*min were calculated in individual RCMs and observed (GriSt) data by averaging data across grid boxes that fall within each region. The numbers of grid boxes and their mean altitudes are summarized in Table 2. Since RegCM has a different orientation of the spatial grid, the regions are slightly modified in this model but the differences are minor (except that

Table 2. Numbers of grid boxes/stations and their mean altitudes in the two regions

	Central lowland (CL)		Central highland (CH)	
RCM run	Number of grids	Altitude [m a.s.l.]	Number of grids	Altitude [m a.s.l.]
hir_ec3	18	264	12	553
rac_ec3	18	264	12	553
rem_ec3	16	315	14	496
reo_ec3	18	264	12	553
rca_ec3	18	261	12	548
rca_bcm	18	261	12	548
rca_hd3	18	261	12	548
rca_ERA	18	261	12	548
GriSt	18	257	12	549

the RegCM model has generally less realistic orography and smaller differences between lowland and higher elevated areas; see also Table 2). Note that the mean elevations of grid boxes in all RCMs except for RegCM and in both regions do not differ by more than 7 m from the mean elevation of the area in the GriSt database. In the case of RegCM, the differences exceed 50 m and are in opposite directions in the two regions.

For estimating extremes (20-year return values) of *T*max and *T*min, the Generalized Extreme Value (GEV) distribution (Coles, 2001) was fitted to samples of annual maxima/minima using the method of L-moments (Hosking, 1990).

2.4. *Classification of atmospheric circulation*

Daily atmospheric circulation characteristics are represented by a classification described in Barry and Carleton (2001) and derived from circulation indices (Jenkinson and Collison, 1977). Flow direction (DIR), flow strength (STR) and flow vorticity (VORT) were calculated from the gridded mean sea level pressure using equations given in Blenkinsop et al. (2009), except that the grid cells in which the sea level pressure data are considered were centred over Central Europe (15°E, 50°N) and the coefficients were adjusted to reflect the dependence of the grid box area on latitude. The equations are summarized in the Appendix.

DIR is divided into four quadrants (northeast 0–90°, southeast 90–180°, southwest 180–270° and northwest 270–360°). For STR and VORT <6, the flow is determined as unclassified (Barry and Carleton, 2001). For |VORT| < STR, the flow is straight; if STR ≤ |VORT| < 2 × STR, a hybrid direction/curvature type is classified; and if |VORT| ≥ 2 × STR, the flow is strongly cyclonic (VORT > 0) or anticyclonic (VORT < 0).

3. Evaluation of RCM simulations

3.1. *Evaluation of basic temperature characteristics in the RCM simulations*

Differences in monthly means of *T*max and *T*min between the control runs of RCMs and the observed gridded data are shown separately for the RCMs driven by the ECHAM5 GCM (Fig. 2), and the RCA RCM with various driving data (GCMs:

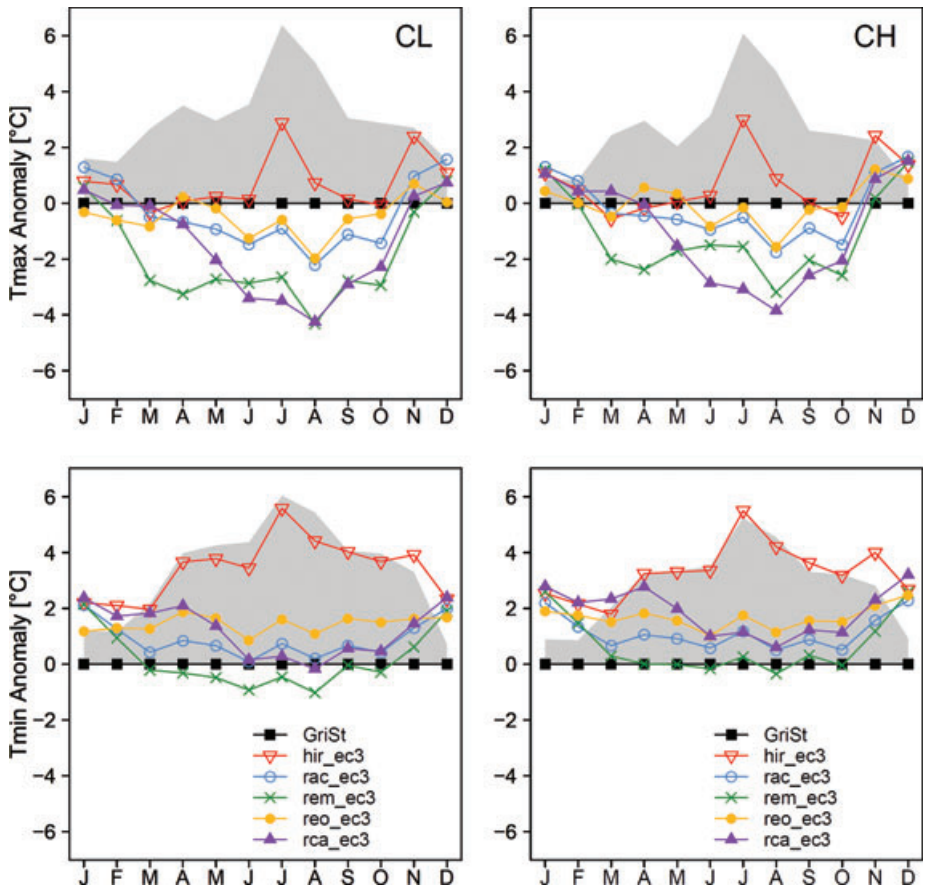

Fig. 2. Mean monthly temperatures in five RCMs driven by the ECHAM5 GCM, shown as anomalies from the observed data (GriSt) for the period 1961–1990 in the CL (left-hand side) and CH (right-hand side) regions. The shaded areas represent the range of differences among the examined RCMs.

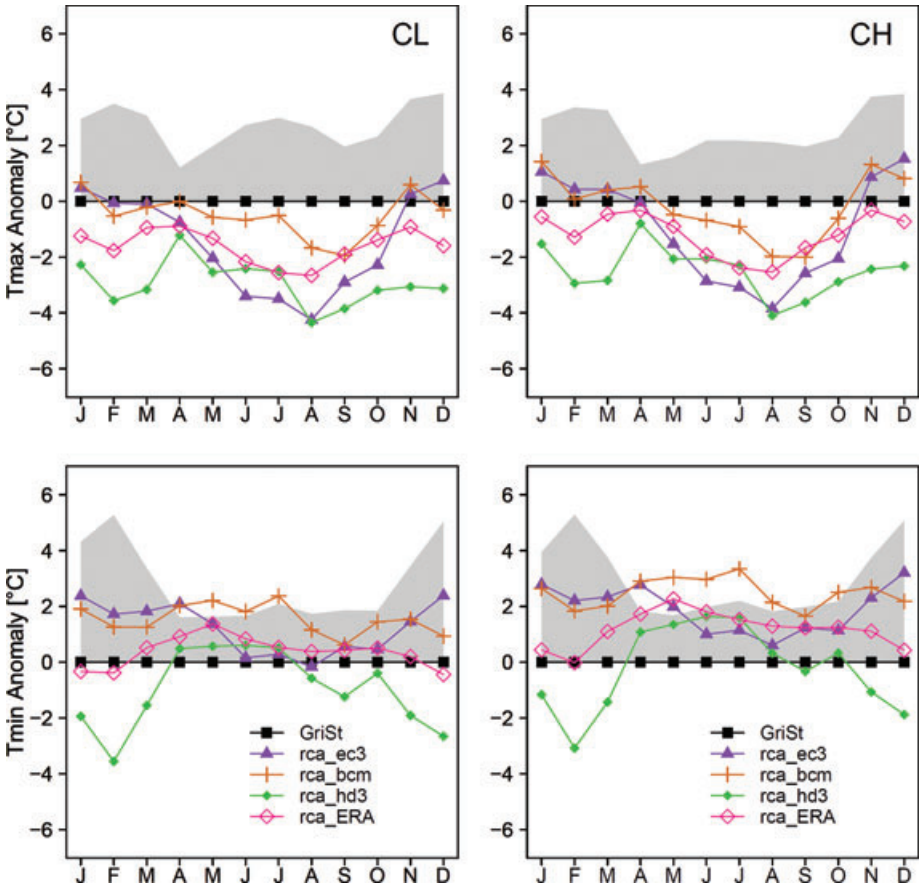

Fig. 3. Same as in Fig. 2 but in four RCA simulations driven by different GCMs and the ERA-40 re-analysis.

ECHAM5, BCM and HadCM3, and the ERA-40 re-analysis; Fig. 3).

While most of the models reproduce some characteristics of the annual cycle of temperatures reasonably well in comparison to that obtained from GriSt, there are many errors in the RCM simulations. Comparison of the left and right panels in Figs 2 and 3 reveals that skills of the individual models are broadly independent of the regions; the differences are much larger between Tmin and Tmax than between the CL and CH regions. The annual cycle of the bias in monthly means has a similar pattern for Tmax and Tmin, except that Tmax tends to be underestimated but Tmin overestimated in most parts of the year. The biases in mean monthly temperatures reach up to +5.5°C for Tmin (in HIRHAM) and −4.5°C for Tmax (in two runs of RCA). The shape of the annual cycle of the bias means that the RCMs driven by ECHAM5 (Fig. 2) tend to have a flatter annual cycle of Tmax and Tmin and underestimate the difference between warm and cold season, except for HIRHAM, which shows the opposite pattern.

The shaded areas in Figs 2 and 3 highlight the range of differences in mean monthly temperatures among the RCMs. All investigated RCMs driven by ECHAM5 (Fig. 2) give Tmax and Tmin very similar in winter (differences between the five RCMs around 1 °C in December–February) whereas in the rest of the year, the mean monthly temperatures differ considerably (by more than 5 °C in July) among the models. A pattern almost opposite appears for a single-RCM driven by several GCMs (Fig. 3): the runs of the RCA model differ in simulations of temperatures more in the cold half than warm half of the year.

The finding that the same driving data produce RCM simulations more similar in winter than summer holds true for simulations of the same set of RCMs driven by the ERA-40 re-analysis, too. Figure 4 shows that differences of mean monthly temperatures between five examined RCMs driven by ERA-40 are also around 1 °C in winter, while they are surprisingly large (up to 4 °C) in summer and autumn. The biases reach up to ±3 °C for some models despite the nearly perfect boundary conditions, which illustrates that the errors of RCM simulations driven by ECHAM5 in summer (Fig. 2) cannot be attributed to the driving data only. The root-mean-square error of mean monthly temperatures, averaged over the five RCMs and two regions, is only slightly larger for simulations driven by ECHAM5 (1.5 °C for Tmax, 1.8 °C for Tmin) than ERA-40 (1.1 °C for Tmax, 1.3 °C for Tmin). Hereafter, 'error of RCM' is used to refer to a given RCM simulation notwithstanding whether it is driven by a GCM or re-analysis.

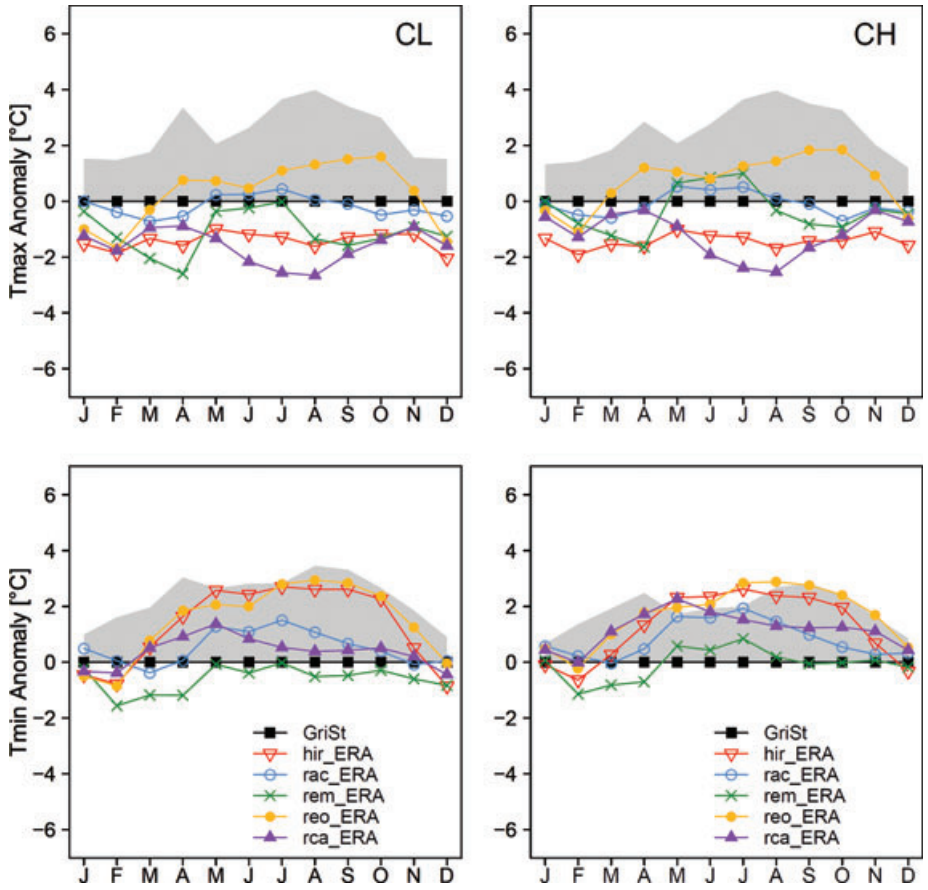

Fig. 4. Same as in Fig. 2 but in simulations driven by the ERA-40 re-analysis. The acronyms used are analogous to those introduced in Table 1.

The prevailing tendency of the RCMs towards too cold *T*max and too warm *T*min is clearly manifested in a pronounced underestimation of the diurnal temperature range (DTR; Fig. 5), which is found for all RCMs and in both regions throughout the year. None of the examined RCMs reproduces the maximum in the annual cycle of DTR that occurs in August; the maximum is shifted to May–July in the RCMs, and even to April in the RCA runs driven by HadCM3 and ERA-40. This may indicate errors in simulating the annual cycle of cloudiness, vertical heat transport or other climate processes represented in RCM parametrizations (e.g. Lenderink et al., 2007; Kyselý et al., 2008) and affecting the difference between daytime and nighttime temperatures. All RCM-simulated mean monthly values of DTR lie outside the 95% confidence intervals of the observed data except for RCA driven by HadCM3 in February (Fig. 5).

Differences in mean seasonal temperatures in control RCM simulations (1961–1990) against the observed data are significant in most RCMs throughout the year (Table 3). The model errors tend to be smallest and least significant for *T*max in MAM (which is in agreement with the result for ALADIN-Climate RCM across the Balkan Peninsula; Kostopoulou et al., 2009), while for *T*min they are almost always significant. There is a rather general tendency towards too cold *T*max in MAM, JJA and SON, as well as too warm *T*min throughout the year.

Spatial patterns of the model errors of mean winter and summer temperatures over the Czech Republic are shown in Figs 6 and 7. The maps illustrate large differences among the RCMs; the patterns as well as magnitude of the bias show little consistency between seasons and variables. In DJF, all five models driven by ECHAM5 show comparable performance and a similar bias: too warm *T*min, and relatively good simulation of *T*max (slight warm bias). In JJA, differences between the RCMs driven by ECHAM5 become much larger: while HIRHAM shows large positive bias of *T*min (+4.5 °C on average over the area), the average bias of *T*min is less than 0.9 °C in RACMO, RegCM and RCA.

Differences among the RCA runs are relatively minor in summer (too cold *T*max and slightly too warm *T*min; Fig. 7). In winter, the differences become larger (Fig. 6): the RCA run driven by HadCM3 simulates too cold *T*max/*T*min (by −2.5 °C/−1.9 °C on average over the area) while the runs driven by ECHAM5 and BCM produce warm biases (around +0.5 °C for *T*max and +2.5 °C for *T*min). This again points to the role of the driving data, which impose strong control on the

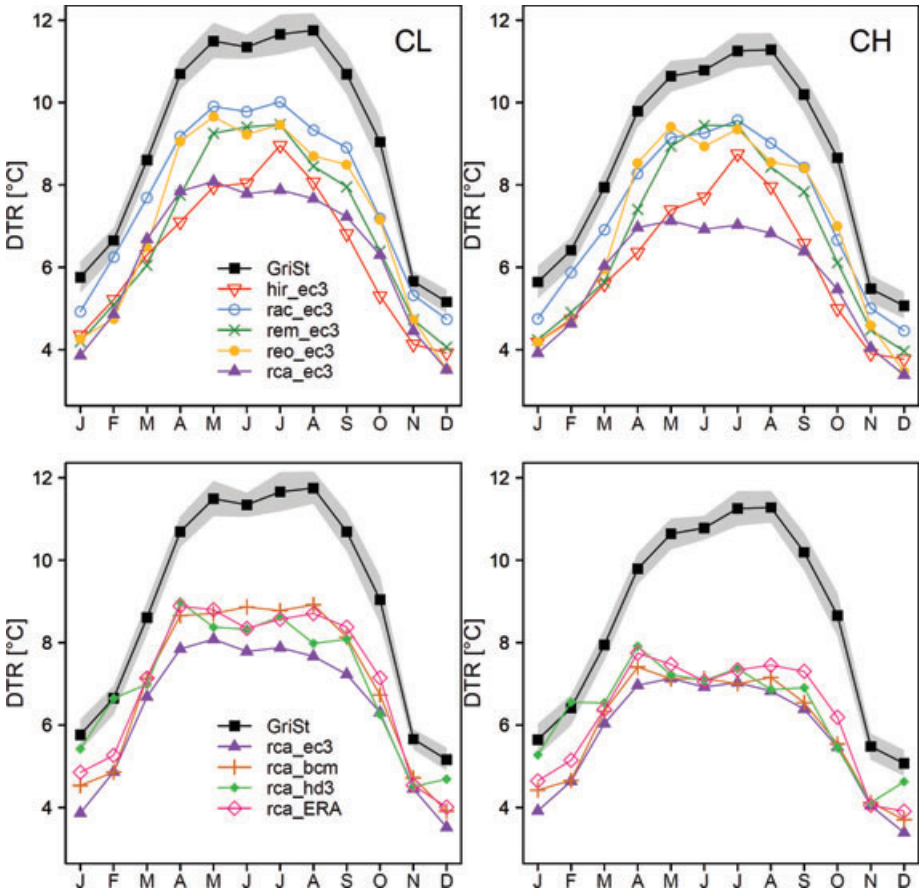

Fig. 5. Mean diurnal temperature range (DTR) in five RCMs driven by the ECHAM5 GCM (top panel) and in four RCA simulations driven by different GCMs and the ERA-40 re-analysis (bottom panel) in comparison to observed data (GriSt). The shaded areas show the 95% confidence interval for the observed data estimated by bootstrapping ($R = 10\,000$).

RCM-simulated temperatures in winter; in summer, the RCM formulation becomes more important.

3.2. *Evaluation of distribution functions of daily temperatures*

The quantile–quantile plots of Tmin in DJF (Fig. 8) show large distortions of the distribution functions in the RCMs and particularly large biases in the lower part of the distribution. Temperatures below the 10% quantile are biased by around 3–4 °C in most RCMs. The bias is positive except for RCA driven by HadCM3, for which the lower tail of Tmin in DJF is too cold. The five RCMs driven by ECHAM5 show remarkably similar errors, which obviously propagate to some extent from the driving GCM. The four RCA simulations with different driving models (bottom row in Fig. 8) produce very different distributions of Tmin if compared one to another. The RCM simulation with the best performance is clearly RCA driven by the ERA-40 re-analysis. This suggests that if the forcing of the RCM simulation by the driving model is 'correct', the RCA RCM is able to provide quite realistic distribution of Tmin in winter (note also much better simulations of mean monthly Tmin in RCMs driven by re-analysis than in runs driven by GCMs in winter, Figs 2–4). The errors in the other simulations of RCA are likely connected with errors in the driving GCM.

For Tmax in JJA (Fig. 9), all RCMs show a better skill for the lower part of the distribution (cold tail) than the upper part (warm tail). The four RCA runs with different driving data display similar tendencies, and in particular a large negative bias for the upper part of the distribution (for above-median Tmax). The only model that has a positive bias of warm extremes is HIRHAM. In contrast to Tmin in DJF, none of the models, including the RCA driven by the re-analysis, produces a temperature distribution close to the observed one for Tmax in JJA. It is noteworthy that the errors in the RCA run driven by ERA-40 are quite similar to the errors in the other runs of RCA driven by GCMs (Fig. 9). This highlights the important role of the RCM formulation and parametrization schemes for surface temperatures in summer (e.g. the soil scheme's sensitivity to drying, Seneviratne et al., 2002).

Figure 10 illustrates that the model errors in the cold tail of Tmin (5% quantile) are typically larger in the cold than warm

Table 3. Evaluation of differences in mean seasonal *T*max and *T*min in control RCM simulations (1961–1990) against the observed data (GriSt) in the two regions

a. *T*max								
	Central lowland (CL)							
RCM run	DJF (°C)	*p*-value	MAM (°C)	*p*-value	JJA (°C)	*p*-value	SON (°C)	*p*-value
hir_ec3	**0.86**	<0.01	−0.01	0.96	**1.26**	<0.01	**0.82**	<0.01
rac_ec3	**1.25**	<0.01	**−0.69**	<0.01	**−1.53**	<0.01	**−0.54**	<0.01
rem_ec3	**0.28**	0.02	**−2.91**	<0.01	**−3.28**	<0.01	**−2.02**	<0.01
reo_ec3	**−0.28**	0.01	−0.26	0.15	**−1.27**	<0.01	−0.08	0.65
rca_ec3	**0.40**	<0.01	**−0.96**	<0.01	**−3.72**	<0.01	**−1.65**	<0.01
rca_bcm	−0.04	0.70	−0.27	0.11	**−0.95**	<0.01	**−0.74**	<0.01
rca_hd3	**−2.96**	<0.01	**−2.31**	<0.01	**−3.10**	<0.01	**−3.37**	<0.01
rca_ERA	**−1.53**	<0.01	**−1.06**	<0.01	**−2.47**	<0.01	**−1.40**	<0.01
	Central highland (CH)							
RCM run	DJF (°C)	*p*-value	MAM (°C)	*p*-value	JJA (°C)	*p*-value	SON (°C)	*p*-value
hir_ec3	**1.00**	<0.01	−0.23	0.21	**1.40**	<0.01	**0.64**	<0.01
rac_ec3	**1.28**	<0.01	**−0.47**	<0.01	**−1.07**	<0.01	**−0.44**	0.01
rem_ec3	**0.91**	<0.01	**−2.03**	<0.01	**−2.09**	<0.01	**−1.49**	<0.01
reo_ec3	**0.46**	<0.01	0.14	0.45	**−0.85**	<0.01	0.28	0.11
rca_ec3	**1.02**	<0.01	**−0.39**	0.02	**−3.27**	<0.01	**−1.26**	<0.01
rca_bcm	**0.79**	<0.01	0.14	0.39	**−1.20**	<0.01	**−0.43**	<0.01
rca_hd3	**−2.23**	<0.01	**−1.90**	<0.01	**−2.83**	<0.01	**−2.99**	<0.01
rca_ERA	**−0.85**	<0.01	**−0.57**	<0.01	**−2.29**	<0.01	**−1.07**	<0.01
b. *T*min								
	Central lowland (CL)							
RCM run	DJF (°C)	*p*-value	MAM (°C)	*p*-value	JJA (°C)	*p*-value	SON (°C)	*p*-value
hir_ec3	**2.22**	<0.01	**3.13**	<0.01	**4.49**	<0.01	**3.87**	<0.01
rac_ec3	**1.81**	<0.01	**0.64**	<0.01	**0.34**	<0.01	**0.79**	<0.01
rem_ec3	**1.69**	<0.01	**−0.34**	<0.01	**−0.80**	<0.01	0.09	0.46
reo_ec3	**1.39**	<0.01	**1.60**	<0.01	**1.19**	<0.01	**1.59**	<0.01
rca_ec3	**2.18**	<0.01	**1.76**	<0.01	0.09	0.20	**0.82**	<0.01
rca_bcm	**1.37**	<0.01	**1.83**	<0.01	**1.78**	<0.01	**1.20**	<0.01
rca_hd3	**−2.71**	<0.01	−0.17	0.24	**0.17**	0.03	**−1.18**	<0.01
rca_ERA	**−0.39**	<0.01	**0.94**	<0.01	**0.58**	<0.01	**0.38**	<0.01
	Central highland (CH)							
RCM run	DJF (°C)	*p*-value	MAM (°C)	*p*-value	JJA (°C)	*p*-value	SON (°C)	*p*-value
hir_ec3	**2.47**	<0.01	**2.78**	<0.01	**4.37**	<0.01	**3.60**	<0.01
rac_ec3	**1.96**	<0.01	**0.88**	<0.01	**0.76**	<0.01	**0.98**	<0.01
rem_ec3	**2.24**	<0.01	0.10	0.45	−0.08	0.27	**0.48**	<0.01
reo_ec3	**2.05**	<0.01	**1.63**	<0.01	**1.31**	<0.01	**1.73**	<0.01
rca_ec3	**2.75**	<0.01	**2.36**	<0.01	**0.92**	<0.01	**1.55**	<0.01
rca_bcm	**2.23**	<0.01	**2.65**	<0.01	**2.82**	<0.01	**2.28**	<0.01
rca_hd3	**−2.03**	<0.01	**0.33**	0.03	**1.18**	<0.01	**−0.36**	0.01
rca_ERA	**0.29**	0.04	**1.70**	<0.01	**1.54**	<0.01	**1.20**	<0.01

Notes: p-value stands for the level at which the difference between the means is significantly different from zero according to the *t*-test. The differences in means significant at the 0.05 level are highlighted in bold.

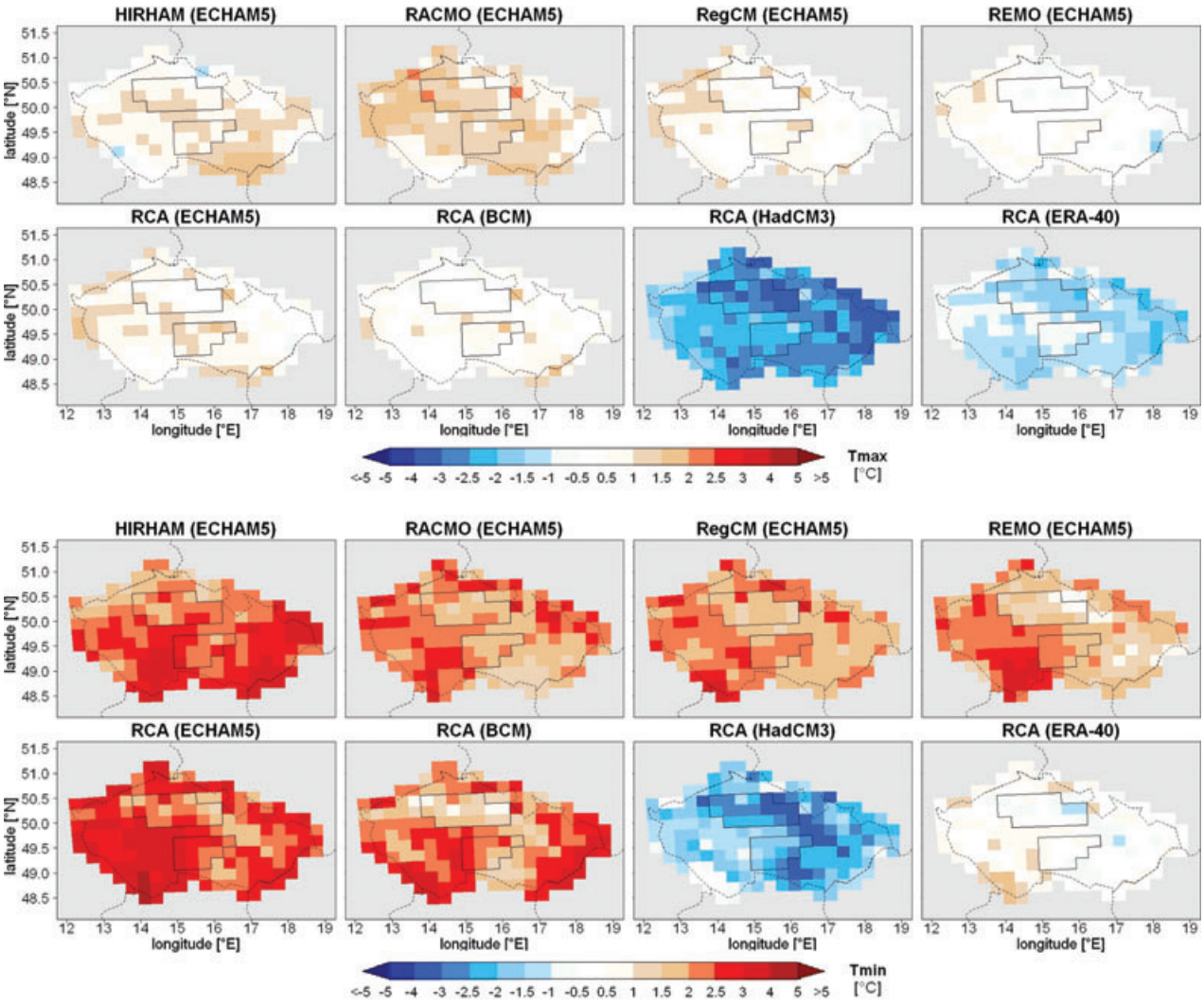

Fig. 6. Differences in mean *T*max (top) and *T*min (bottom) between control RCM simulations and observed data (GriSt) in DJF.

season while the opposite is true for the warm tail of *T*max (95% quantile). This means that the model errors tend to be largest for those tails of the temperature distributions that are particularly relevant for impacts, that is, cold extremes in winter and warm extremes in summer, which may impose some limitations also on the credibility of their scenarios for future time horizons and use of these scenarios in impact studies.

3.3. Evaluation of low and high quantiles of daily temperatures and extremes

Since warm extremes in summer and cold extremes in winter are most closely associated with environmental and societal impacts of surface temperature conditions, we focus on the reproduction of tails of the distributions of *T*max in summer and *T*min in winter and the respective extremes in this section.

The models' errors in 20-yr return values (estimated using the GEV distribution) and low quantiles of *T*min in DJF and high quantiles of *T*max in JJA are summarized in Table 4. For *T*max in JJA, two RCMs—RACMO and REMO—show a good skill in reproducing the upper tail (the bias is smaller than 1 °C in most characteristics). The bias in RegCM is small only in the CH region while it becomes pronounced in the CL region. This is related to a combination of the prevailing cold bias and smoothed orography in the model (see Table 2), which has too high elevation of the lowland region (and hence large cold bias) but too low elevation of the highland region (and hence the cold bias is reduced). In the other RCMs, the typical bias in the upper tail exceeds 3 °C (in absolute value), and it is negative except for HIRHAM. A remarkably large cold bias in the 20-yr return level of *T*max is found also for RCA driven by the ERA-40 re-analysis (between 4 and 5 °C). This is in accordance with findings of Nikulin et al. (2010), who showed that the bias of the 20-yr return level of *T*max in RCA driven by ERA-40 is larger and more significant than the mean bias in six RCA runs driven

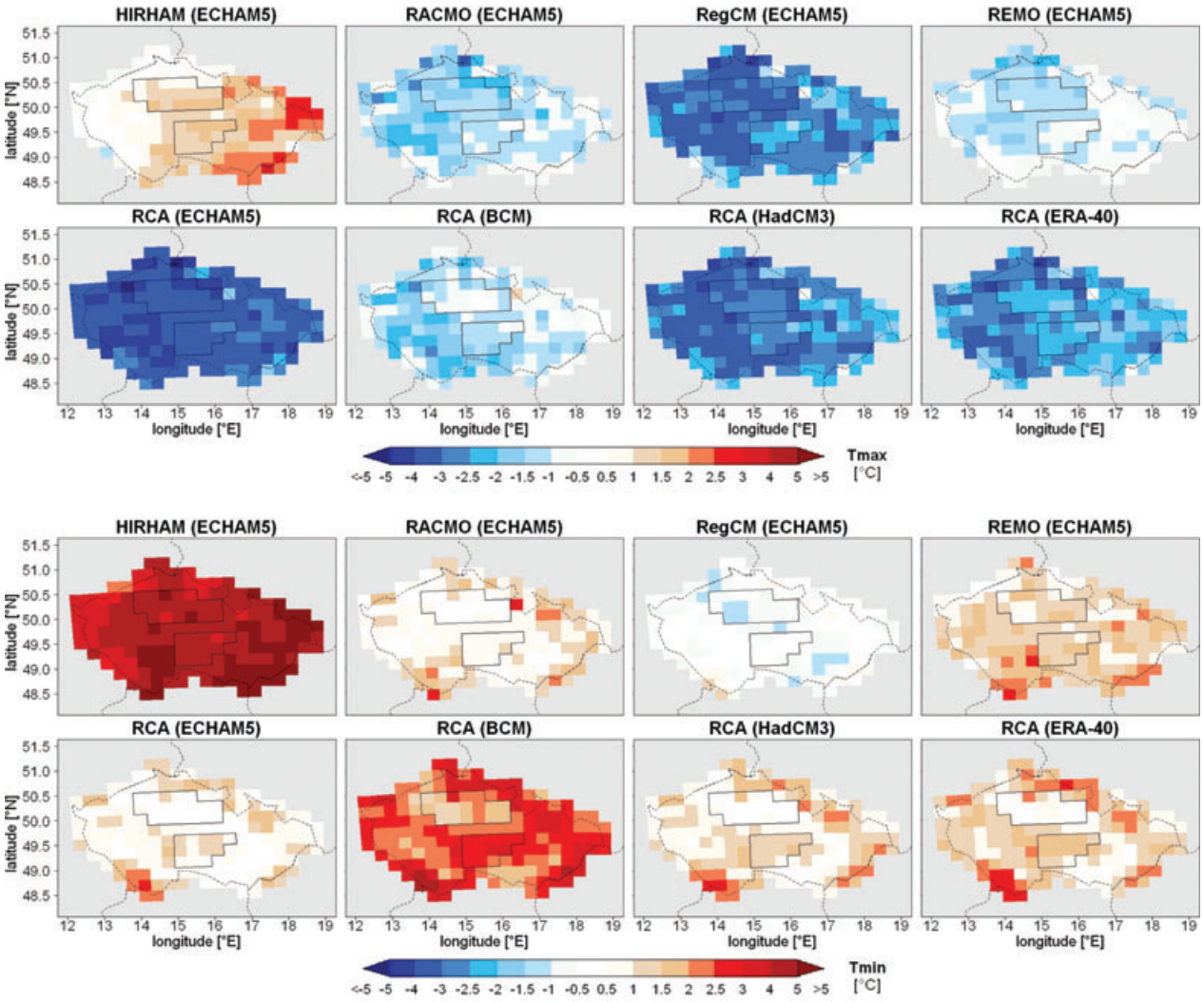

Fig. 7. Same as in Fig. 6 but for JJA.

by different GCMs in Central Europe (in that study, RCA runs with ∼50 km resolution were examined).

For *T*min in DJF, the lower tail is captured in the RCA driven by the ERA-40 re-analysis (Table 4). The small bias of the 1% quantile and the 20-yr return value of *T*min in REMO is due to compensating effects of a warm bias in *T*min (which is quite pronounced for the 5% quantile up to around the median of the distribution; cf. the upper right graph in Fig. 8) and a heavier lower tail of the distribution of *T*min. Except for REMO, the errors in the lower tail of *T*min are pronounced in the other RCMs driven by GCM data, and they are positive with the exception of the RCA driven by HadCM3, which shows a large negative bias.

If warm and cold extremes are considered together, the only model reproducing both the warm and cold tails of the temperature distributions is REMO (Table 4). A rather general (although not uniform) tendency of the other RCMs is to underestimate the severity of extremes, that is, to have a warm bias for cold extremes while a cold bias for warm extremes.

3.4. *Atmospheric circulation simulated in RCMs*

Frequencies of circulation types in the RCM simulations are compared in Table 5 with those derived from the ERA-40 re-analysis over 1961–1990. Although most of the models capture at least some circulation characteristics, the differences among the RCMs are large. This holds true even within the set of RCMs driven by the same GCM (ECHAM5), in which one RCM—HIRHAM—develops circulation that deviates from the other RCMs with the same driving data. HIRHAM has a much larger frequency of southwesterly types at the expense of northwesterly types in both seasons, and it has a smaller frequency of anticyclonic types and larger frequencies of cyclonic types and straight flow in winter (Table 5).

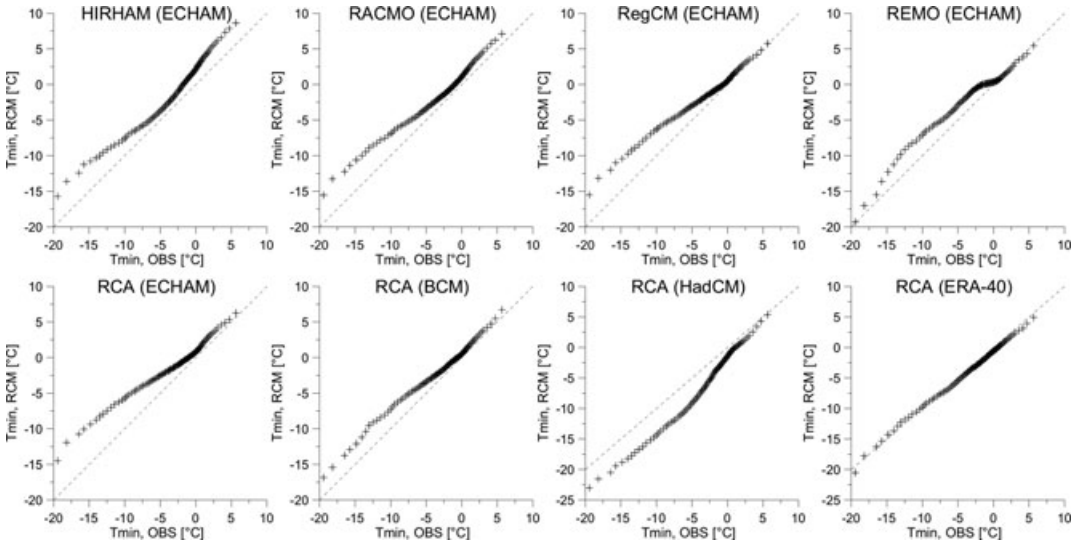

Fig. 8. Quantile–quantile plots of *T*min in DJF for RCM simulations against observed data (GriSt) in the CL region. The 1 to 99% quantiles (marked with crosses) were calculated as empirical quantiles from the distribution function.

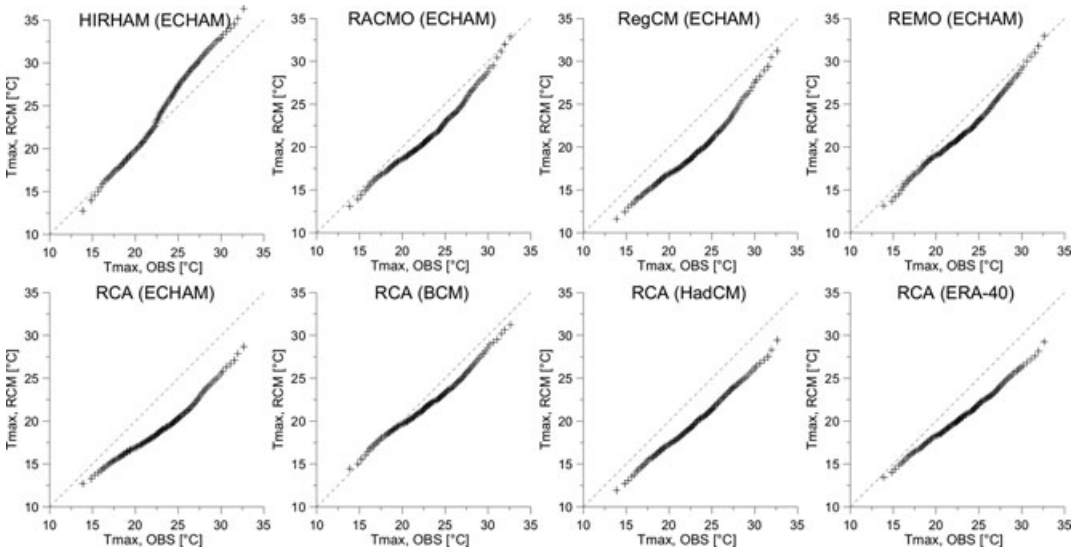

Fig. 9. Same as in Fig. 8 but for *T*max in JJA.

Rather general features of the models' errors in circulation characteristics, common to all RCMs, are overestimated straight flow in both seasons plus underestimated anticyclonic and overestimated cyclonic types in winter (Table 5). Note that the atmospheric flow is completely distorted in the RCA driven by BCM in summer, which makes results of this particular run somewhat suspicious: 79% of days have a flow with the easterly component compared to 45% in ERA-40, and northwesterly and southwesterly flows as well as anticyclonic types are 2–3 times less frequent than in ERA-40. Westerly types (NW and SW considered together) are overestimated in winter in all model runs except for RCA driven by HadCM and ERA-40. The strong overestimation of westerly types at the expense of easterly types over Europe in winter seems to be a rather general feature of climate models, as it has been reported by Blenkinsop et al. (2009) for all examined PRUDENCE RCMs, by Demuzere et al. (2009) for ECHAM5 GCM, and by Kjellström et al. (2011) for several RCA runs driven by different GCMs (including ECHAM5).

4. Links between biases in surface temperature and atmospheric circulation

4.1. Relationship between circulation types and surface temperature

To illustrate the relationships between circulation types and surface temperatures, the daily *T*max and *T*min values were converted into anomalies by subtracting their annual cycles over the

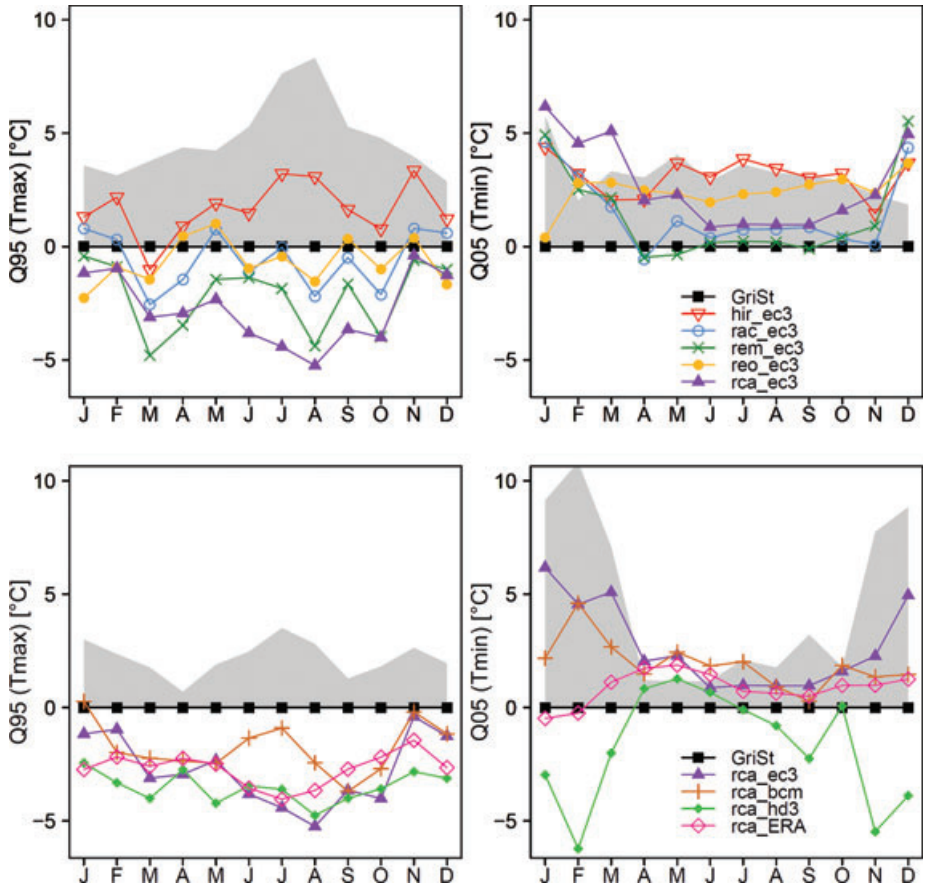

Fig. 10. The 95% quantile of *T*max (Q95, left-hand side) and the 5% quantile of *T*min (Q05, right-hand side) in five RCMs driven by the ECHAM5 GCM (top panel) and four RCA simulations driven by different GCMs and the ERA-40 re-analysis (bottom panel), shown as anomalies from the observed data (GriSt) for the period 1961–1990 in the CL region. The shaded areas represent the range of differences among the examined RCMs.

baseline period of 1961–1990 (smoothed with 11-day running means). Mean daily *T*max and *T*min anomalies on days falling into each circulation/directional type are shown for the observed data in Table 6, and they are compared with those derived for RCMs in Fig. 11.

The influence of the direction from which the flow is advected is large, particularly for *T*max. In winter, a flow with the easterly component (SE, NE) is generally linked to cold temperature anomalies and a flow with the westerly component (SW, NW) to warm anomalies; in summer, the pattern is shifted by 90° and a flow with the northerly component (NW, NE) leads to cold anomalies and a southerly flow (SW, SE) to warm anomalies. Strongly cyclonic flow is linked to cold *T*max anomalies in both seasons and smaller cold/warm *T*min anomalies in winter/summer. Strongly anticyclonic flow is linked to warm *T*max anomalies in both seasons and cold *T*min anomalies in summer. Average temperature anomalies associated with the hybrid flow are minor and insignificant, as expected (Table 6).

The observed links are reproduced reasonably well in the RCMs (Figs 11 and 12). Colours in Fig. 12 illustrate the mean temperature anomaly (with respect to the mean annual cycle in a given RCM) linked to each circulation/directional type. In winter, an easterly flow, cyclonic types and straight flow are associated with negative anomalies of *T*max while a southwesterly flow and anticyclonic types with positive anomalies in all RCMs (Figs 11 and 12). In summer, a northerly flow and cyclonic types are characterized by negative anomalies of *T*max while a southerly flow and anticyclonic types by positive anomalies in all RCMs. In general, the circulation characteristics are much more closely linked to anomalies of *T*max than *T*min for the observed data, especially in summer, and this is captured also in the RCMs (Table 6, Fig. 11).

4.2. *Influence of atmospheric circulation on temperature biases in the RCMs*

Comparing biases in temperature and circulation characteristics in the RCMs yields some insight into sources of the errors in simulated surface temperatures, and it shows that the largest temperature biases are usually linked to corresponding biases in the simulation of large-scale circulation.

Table 4. Differences in extremes (20-yr return values, r.v.) and low (1% and 5%) and high (95% and 99%) quantiles of daily temperatures in control RCM simulations (1961–1990) against the observed data (GriSt) in the two regions

	Central lowland (CL)					
RCM run	*T*min, DJF (°C)			*T*max, JJA (°C)		
	20-yr r.v.	Q01	Q05	Q95	Q99	20-yr r.v.
hir_ec3	3.38	3.74	4.03	3.03	3.70	4.24
rac_ec3	4.28	3.90	4.23	**−1.09**	**0.27**	**0.03**
rem_ec3	3.36	3.94	4.40	−2.30	**−1.41**	**−1.86**
reo_ec3	**0.20**	**0.12**	2.56	**−0.61**	**0.35**	**0.05**
rca_ec3	5.66	4.96	5.46	−4.31	−3.95	−5.01
rca_bcm	**1.43**	2.59	2.72	**−1.42**	**−1.37**	−2.87
rca_hd3	−3.13	−3.59	−3.99	−3.84	−3.19	−3.07
rca_ERA	**−0.37**	**−1.09**	**0.54**	−3.77	−3.36	−4.12
	Central highland (CH)					
RCM run	*T*min, DJF (°C)			*T*max, JJA (°C)		
	20-yr r.v.	Q01	Q05	Q95	Q99	20-yr r.v.
hir_ec3	**1.71**	2.06	3.47	2.92	3.77	3.38
rac_ec3	**1.41**	2.03	3.09	**−0.31**	**0.59**	**−0.03**
rem_ec3	2.25	3.42	4.25	**−0.86**	**−0.15**	**−0.45**
reo_ec3	**−0.43**	**−0.39**	2.41	**−0.15**	**0.39**	**−0.80**
rca_ec3	2.47	3.33	5.09	−3.61	−3.56	−4.45
rca_bcm	2.03	2.11	3.12	−2.42	−2.70	−4.84
rca_hd3	−4.37	−4.24	−4.06	−3.99	−2.49	−3.20
rca_ERA	**0.12**	**0.35**	**0.89**	−3.55	−3.65	−4.91

Note: Absolute values of the bias less than 2 °C are marked in bold.

4.2.1. Winter (DJF). A conspicuous common feature of most RCMs (all five runs driven by ECHAM5, as well as the RCA run driven by BCM) is a warm bias (larger for *T*min than *T*max); the RCA driven by HadCM3 clearly stands out as it has a large cold bias (Figs 6 and 8). All six model runs with the warm bias overestimate flows with the westerly component (NW, SW; Table 5) at the expense of flows with the easterly component (NE, SE). This points to a too strong influence of the Atlantic Ocean (an advection of maritime, relatively warm air masses) on surface temperatures and reduced continental influences. Table 6 shows that flow with the westerly (easterly) component is linked to pronounced warm (cold) temperature anomalies in winter. The idea that the circulation-related bias is important for winter temperatures is supported by the fact that the only two RCM simulations with cold bias (the RCA runs driven by HadCM3 and ERA-40) display the opposite pattern with overestimated northeasterly (cold) flow at the expense of southwesterly (warm) flow.

A general feature of all the RCMs is that they underestimate (overestimate) the frequency of strongly anticyclonic (strongly cyclonic and straight) flow in winter (Table 5). Underestimation of anticyclonic flow (linked to warm anomalies of *T*max, Fig. 12) and overestimation of cyclonic and straight flows (linked to cold anomalies of *T*max) support relatively colder *T*max in comparison to *T*min, since the warm/cold effect of strongly anticyclonic/cyclonic days is much larger on *T*max than *T*min anomalies (cf. Table 6). This circulation-related bias is likely to contribute to the underestimation of DTR that is universal for the examined RCMs.

Figure 5 shows relatively smaller underestimation of the simulated DTR in winter by RACMO in comparison to most other models. The underestimation of DTR may be supported by overestimation of the frequencies of straight flow (too strong advection resulting in reduced *T*max), which is found in all RCMs except RACMO (Table 5).

4.2.2. Summer (JJA). Differences in atmospheric circulation among the RCMs are larger (Table 5) and the relationship between errors in circulation and in surface temperatures is somewhat less obvious in summer than winter.

Similarly to winter, all RCMs overestimate the straight flow days (associated with strong advection, Table 5), which may be

Table 5. Relative frequencies of circulation and directional types (in %) for classification calculated from circulation indices (Barry and Carleton, 2001; Blenkinsop et al., 2009) for the RCM simulations and the ERA-40 re-analysis over 1961–1990

DJF	Straight	Cyclonic	Anticyclonic	Hybrid	Uncl.	NW	SW	SE	NE
ERA40	27.6	8.0	39.0	21.2	4.2	28.0	38.2	21.6	12.2
hir_ec3	38.3	12.7	18.5	27.9	2.7	23.2	48.1	16.1	12.6
rac_ec3	28.0	9.2	33.9	25.3	3.6	32.8	38.7	15.7	12.8
rem_ec3	31.0	11.1	28.9	26.6	2.4	36.8	38.1	13.3	11.7
reo_ec3	30.0	8.9	31.6	26.4	3.1	32.9	39.3	15.9	11.9
rca_ec3	30.1	10.2	29.0	26.5	4.2	33.0	39.5	15.1	12.4
rca_bcm	30.4	8.3	31.2	24.2	5.9	20.4	55.4	13.3	10.9
rca_hd3	29.7	15.2	23.9	25.9	5.3	29.8	34.9	19.0	16.3
rca_ERA	29.5	11.6	30.7	23.2	5.1	32.3	33.2	17.1	17.4
JJA	Straight	Cyclonic	Anticyclonic	Hybrid	Uncl.	NW	SW	SE	NE
ERA40	30.9	7.2	13.0	22.1	26.8	27.9	27.1	19.4	25.5
hir_ec3	40.5	3.8	17.6	27.8	10.3	27.2	52.8	12.4	7.5
rac_ec3	36.4	6.3	13.9	24.8	18.6	37.8	26.9	12.6	22.7
rem_ec3	44.0	4.5	14.0	23.6	13.9	42.5	31.6	9.4	16.6
reo_ec3	39.4	7.4	13.1	25.4	14.7	39.2	29.7	11.7	19.3
rca_ec3	40.4	6.6	13.0	25.2	14.7	41.7	30.3	10.1	17.9
rca_bcm	33.2	16.5	4.2	21.1	25.0	9.4	11.8	41.2	37.6
rca_hd3	34.7	10.3	10.1	22.1	22.7	22.4	27.0	26.2	24.4
rca_ERA	31.8	8.7	11.7	23.0	24.9	31.4	24.9	15.8	27.9

Note: Details on the classification are given in Section 2.4.

Table 6. Mean daily *T*max and *T*min anomalies on days falling into individual circulation types over 1961–1990

DJF	Straight	Cyclonic	Anticyclonic	Hybrid	NW	SW	SE	NE
*T*max (°C)	−0.4	−1.1*	0.7*	−0.1	1.6*	1.0*	−2.2*	−3.2*
*T*min (°C)	0.0	−0.4	0.0	0.1	1.9*	0.9*	−2.4*	−3.1*
JJA	Straight	Cyclonic	Anticyclonic	Hybrid	NW	SW	SE	NE
*T*max (°C)	−0.4*	−2.3*	0.8*	−0.1	−2.5*	1.5*	3.1*	−1.1*
*T*min (°C)	0.0	0.6*	−0.9*	−0.2	−0.6*	0.1	0.6*	0.1

Notes: The values were calculated for GriSt temperature data in the CL region and airflow indices from the ERA-40 sea level pressure data. Symbol * denotes the anomalies significantly different from zero at the 0.05 level; the critical values were estimated by block bootstrapping ($R = 10\,000$, the same number and length of sequences of days falling into given types were resampled).

one of the reasons for generally colder *T*max in the RCMs and the underestimation of DTR (Fig. 5).

HIRHAM is the model with the largest warm bias in summer (Figs 6 and 12). This may partly be explained by the noticeable overestimation of southwesterly flow associated with large positive temperature anomalies (Fig. 12): southwesterly flow is simulated on 53% of summer days by HIRHAM in comparison to 27% in the ERA-40 data (and 12–32% in the other RCM simulations; Table 5). The large warm bias in the upper tail of *T*max (Fig. 9) and extremes (Table 4) in HIRHAM is obviously related to this circulation bias with enhanced southwesterly flow and warm advection. The frequency of northeasterly flow, associated with negative *T*max anomalies, is for HIRHAM only about a quarter of that for ERA-40 re-analysis (Table 5). The peculiarity of HIRHAM as to circulation statistics over Central Europe is surprising also in comparison to similar characteristics in the other RCMs driven by ECHAM5. This suggests that HIRHAM is the only RCM to considerably modify circulation patterns relative to the driving GCM.

The RCA run driven by BCM is relatively warmer in comparison to the other RCA runs in summer, which is also linked to its distorted circulation (see Section 3.4 and Table 5) and mainly pronounced overestimation (underestimation) of the southeasterly (northwesterly) flow that is generally connected with large positive (negative) temperature anomalies in summer (Fig. 12).

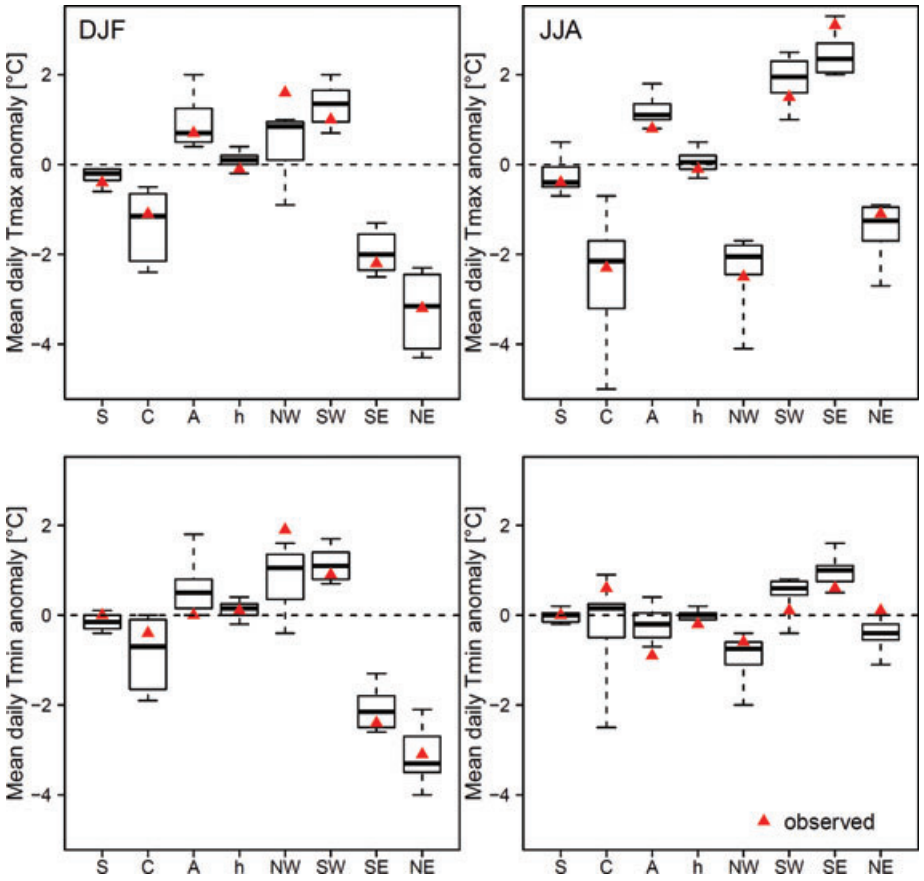

Fig. 11. Mean daily *T*max and *T*min anomalies on days falling into individual circulation types over 1961–1990 calculated for the CL region and airflow indices from the ERA-40 sea level pressure data (triangles) and for eight RCMs (shown as box plots). S, straight; C, cyclonic; A, anticyclonic; h, hybrid; NW, northwesterly; SW, southwesterly; SE, southeasterly; NE, northeasterly flow.

The two examples (HIRHAM and RCA driven by BCM) point out the influence of overestimating flow with the southerly component on the bias of surface temperatures in the RCM simulations in summer. The frequency of northerly (cold) flow is enhanced at the expense of southerly (warm) flow in most other RCMs in comparison to the re-analysis (Table 5), which suggests that the prevailing tendency towards cold bias of *T*max (Figs 7 and 12) is linked to this circulation bias. Note also that the relationship to circulation is much stronger for *T*max than *T*min in summer (Table 6, Fig. 12; cf. similar findings in Blenkinsop et al., 2009, for the United Kingdom). That is why the cold circulation-related bias is manifested mainly for *T*max (Fig. 7) while *T*min (with prevailing warm bias) is related more to land–atmosphere coupling and vertical moisture and energy fluxes.

5. Discussion

5.1. Role of the driving model

In winter, all investigated RCMs driven by ECHAM5 give mean monthly/seasonal *T*max and *T*min (Figs 2 and 6) as well as shapes of the distribution function (Fig. 8) that are very similar. This suggests an important role of the driving model in governing surface temperature distributions in cold season. In summer, on the other hand, the five RCM simulations driven by ECHAM5 differ substantially in all temperature characteristics. This is demonstrated for mean monthly temperature also in simulations driven by re-analysis (Fig. 4). An opposite pattern is found for runs of the RCA RCM with different driving data: they vary in temperature characteristics less in the warm than cold part of the year (cf. Fig. 8 versus Fig. 9). In other words, the RCM formulation is more important in summer than in winter while the opposite holds for the role of the driving GCM. This is in line with one's expectation as well as with other studies (e.g. Holtanová et al., 2010), but the given ensemble of RCMs illustrates this pattern particularly well. The more important role of driving data in winter than summer is supported by the fact that RCM circulation characteristics are influenced by the driving data (GCM/re-analysis) more in winter than summer; a larger spread in circulation characteristics among models in summer has been reported by van Ulden et al. (2007) and Sanchez-Gomez et al. (2009) for the PRUDENCE and ENSEMBLES RCMs.

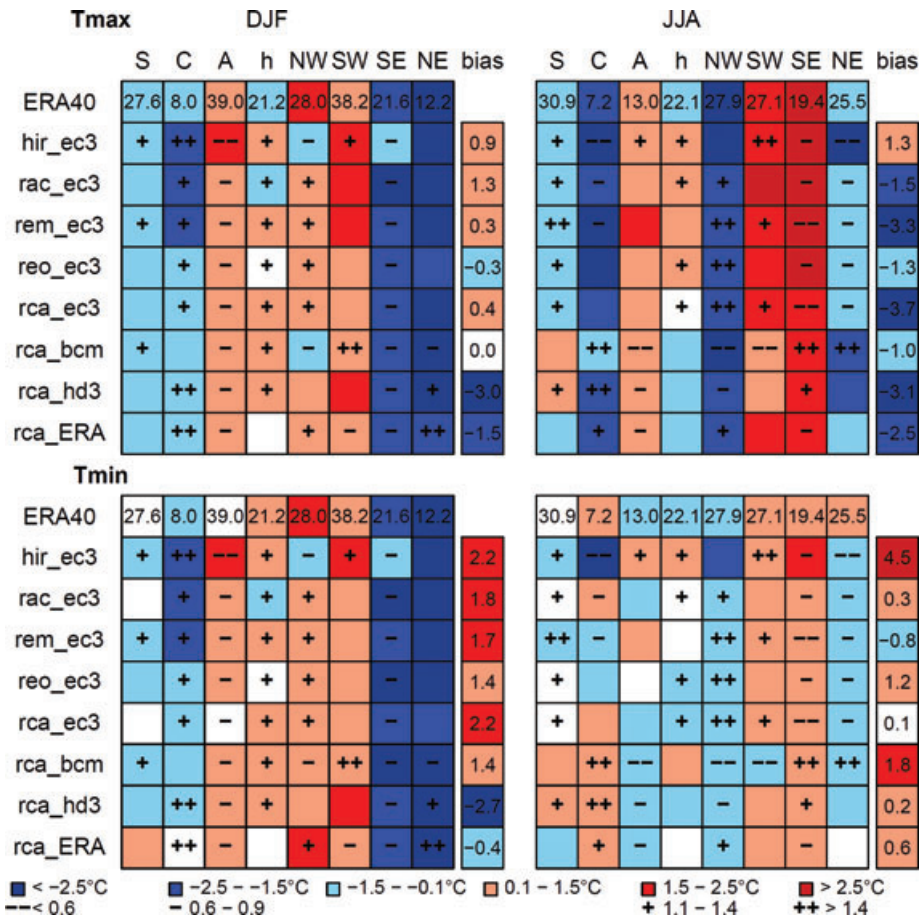

Fig. 12. Overview of temperature anomalies (represented by colours) on days falling into individual circulation types and biases in frequencies of circulation types, for observed and RCMs data, in the CL region over 1961–1990. Total temperature biases (in °C) in given seasons and for given variables are shown in the right columns. Relative frequencies of types (in %) for observed data (ERA-40) are shown in the first row of panels. Symbols + and – indicate the ratio between simulated and observed frequencies of the types (see legend).

The general tendency to produce distorted distributions of *T*min in all RCMs driven by ECHAM5 in winter, with large overestimation in the lower parts of the distributions (Fig. 8), is likely to originate in the driving data as well, since it is reduced or disappears for RCA simulations other than the one driven by ECHAM5. RCA driven by the ERA-40 re-analysis is the model run with the best performance as to the distribution of *T*min in winter, which suggests that the RCA RCM is able to provide quite realistic winter *T*min if the forcing by the driving model is correct. Simulations of other RCMs driven by re-analysis also produce monthly *T*min in winter close to observations. The errors in RCM simulations driven by GCM data in winter seem to be closely connected with errors in the driving GCM. In summer, on the other hand, the RCA run driven by re-analysis produces errors and distribution of *T*max similar to those of the other RCA runs (Fig. 9). This highlights the important role of an RCM (and its inner configuration and parametrization) for modelling surface temperatures in summer.

5.2. *Temperature extremes*

The examined RCMs suffer from generally larger errors in simulating temperature extremes than central parts of the temperature distributions (cf. similar results reported for the PRUDENCE RCMs by Kjellström et al., 2007 and Kyselý et al., 2008). We find that the errors tend to be largest for those tails of the temperature distributions that are particularly relevant for impacts (lower tails of *T*min in winter and upper tails of *T*max in summer); similar results were reported by Jacob et al. (2007) for the PRUDENCE RCMs. The biases reach up to 5 °C (for the 20-yr return values, Table 4) and they differ by sign among the RCMs. As shown by Nikulin et al. (2010), the biases of the 20-yr return temperatures in RCA runs are less significant and smaller in Central Europe compared, for example, to Scandinavia where they reach up to 10 °C and more. The large errors as well as large variability among the models may limit the credibility of RCMs in simulating extreme temperature events in future climate scenarios. Because some errors in the distribution functions

propagate from the driving GCM (Fig. 8 clearly reveals similar errors in the lower tail of *T*min in all five RCMs driven by ECHAM5), it is also necessary to employ RCMs with different driving models and boundary conditions in constructing climate change scenarios.

Our results show that only one RCM (REMO) captures reasonably well both warm and cold tails of the temperature distributions in Central Europe. When mean temperatures are considered, however, the results for REMO are more biased (cf. Tables 3 and 4), so the relatively good performance for extremes is due to some compensating effects that influence the simulated temperature distributions.

5.3. Links between biases in temperature and atmospheric circulation

Observed and GCM- or RCM-simulated relationships between surface air temperature and atmospheric circulation, described by circulation indices, have been examined mainly for the United Kingdom (Osborn et al., 1999; Turnpenny et al., 2002; Blenkinsop et al., 2009). We find that a simple classification scheme derived from the same set of indices characterizing flow direction, strength and vorticity is useful for examining links between circulation and temperature biases in climate model simulations also in Central Europe, that is, in an area where continental influences become more important relative to Western Europe and the United Kingdom. Comparing errors in circulation and surface temperatures yields insight into sources of the temperature biases in individual RCMs.

The links to circulation differ noticeably depending on season and for *T*max and *T*min; they are generally much more pronounced for *T*max (Fig. 11). The examined RCMs reproduce the observed relationships fairly well. Since some circulation types are linked to large temperature anomalies, the deficiencies in simulating atmospheric circulation in RCMs (cf. Table 5) produce biases in simulated surface temperature distributions. Stronger advection in RCMs and especially the direction of the advected flow play the most important roles. Warm advection is associated with westerly flow in winter (i.e. mild and moist air is advected from the North Atlantic). Overestimated zonal flow in all RCMs driven by ECHAM5 contributes to their warm bias while the pronounced cold bias of the RCA run driven by HadCM3 is related to underestimation of the zonal flow and overestimation of the cold northeasterly flow. In summer, warm advection is associated with southerly flow. That may at least partly explain the warm bias in HIRHAM and RCA driven by BCM, since these models overestimate the warmer southerly flow at the expense of the northerly flow.

The deficiencies in simulating large-scale circulation (especially the overestimated advection) could also partly explain the substantial underestimation of the DTR found in all RCMs throughout the year. A shift of maximum in its annual cycle to late spring—early summer suggests, however, that other errors in simulating climate processes affecting the difference between daytime and nighttime temperatures that are rather general for the examined models play roles, and these need to be identified for further development of the models in follow-up studies.

6. Conclusions

Evaluation of daily maximum (*T*max) and minimum (*T*min) temperatures in an ensemble of high-resolution RCM simulations of recent climate against a data set interpolated from a high-density station network in the Czech Republic shows large biases in mean monthly and seasonal temperatures (reaching up to +5.5 °C and –4.5 °C) as well as in tails of the distributions of daily temperatures. The biases are usually larger for extremes than central parts of temperature distributions, and for those tails of the distributions that are particularly relevant for impacts, that is, cold extremes in winter and warm extremes in summer. Substantial underestimation of DTR is detected in all RCMs throughout the year (reaching up to 4 °C in summer in some RCM runs), and the maximum of the annual cycle of DTR is shifted from August to spring or early summer in all RCMs. Since we find that (i) RCMs driven by the same driving data give temperature biases very similar in winter (differences among the five RCMs around 1 °C) whereas in the rest of the year, the mean monthly temperatures differ considerably among the models (by more than 5 °C in July), and (ii) the runs of the same RCM with different driving data differ in simulation of temperatures more in the cold half than warm half of the year, we infer that an RCM's formulation plays a much more important role in summer whereas in winter the RCM performance is closely linked to the driving data.

Some features of the temperature biases of RCMs may be related to deficiencies in the simulation of large-scale atmospheric circulation. The links of temperature anomalies to circulation types differ noticeably depending on season and for *T*max and *T*min. We show that the observed relationships are reproduced quite well in the examined RCMs, so an overestimation (underestimation) of circulation types that are associated with significant temperature anomalies may produce large temperature biases. Potential sources of warm and cold biases of RCMs are too strong advection and overestimation of westerly flow at the expense of easterly flow in most RCMs, and wrong simulation of frequencies of days with anticyclonic, cyclonic and straight flows. Some deficiencies in the simulation of atmospheric circulation probably contribute also to the underestimated DTR in the examined RCMs.

There are several open issues that deserve further investigation, for example, why the HIRHAM RCM develops circulation that substantially deviates from all other RCMs with the same driving data, and thus obviously considerably modifies circulation patterns relative to the driving GCM. Future studies should also address in more detail the contribution of the driving GCM data (including circulation patterns) to the RCM errors.

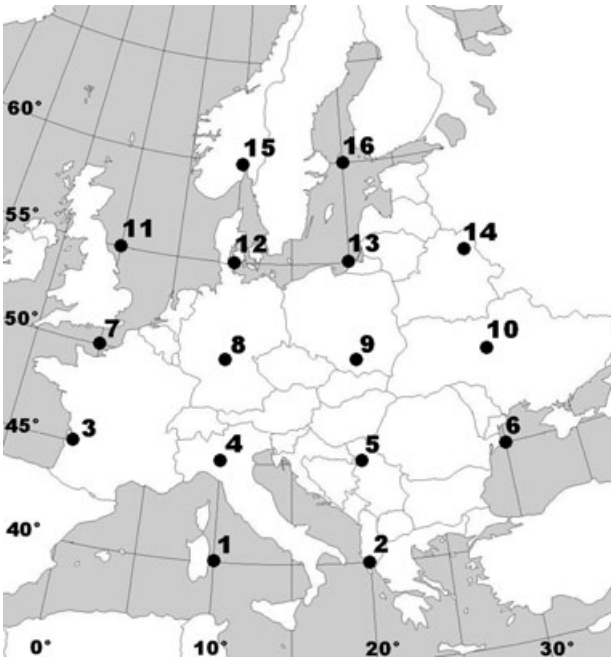

Fig. 13. Grid points used to construct the airflow indices for Central Europe.

A realistic reproduction of the large-scale atmospheric circulation in control RCM and GCM simulations is very important for the use of these models in constructing scenarios of possible future climate. As shown by Kjellström et al. (2011), the spread in the results of a single RCM (RCA) is largely dependent on the choice of GCMs, that is, the choice of the driving data (and circulation patterns). The skill of the models in capturing the atmospheric circulation and the links between circulation and surface air temperature (as well as other meteorological variables) needs to be examined more thoroughly in GCM and RCM evaluation studies, and the findings may also be used to 'weight' GCM/RCM data in constructing future climate change scenarios. Scenarios based on models with a considerably biased circulation in the control climate (such as RCA driven by BCM in this study) should be given very low weights since their climate is unrealistic, and this is likely to hold for future projections as well.

7. Acknowledgments

The study was supported by the Czech Science Foundation under project P209/10/2265. The RCM data used in this work were funded by the EU FP6 Integrated Project ENSEMBLES (Contract number 505539). Special thanks are due to P. Štěpánek, Czech Hydrometeorological Institute, Brno, for calculating and providing the GriSt daily gridded data set.

8. Appendix

The airflow indices are calculated using grid points shown in Fig. 13.

The flow strength is the total resultant westerly w and southerly s flow.

$$\mathrm{STR} = \sqrt{w^2 + s^2}. \tag{A1}$$

The westerly (zonal) component of the geostrophic surface wind calculated as the pressure gradient between 45°N and 55°N represents the westerly flow w.

$$w = 0.5\ (p[4] + p[5]) - 0.5\ (p[12] + p[13]). \tag{A2}$$

The southerly (meridional) component of the geostrophic surface wind represented by the pressure gradient between 10°E and 20°E is the southerly flow s.

$$\begin{aligned} s = {} & 1.56\ (0.25\ (p[13] + 2\ p[9] + p[5]) \\ & - 0.25\ (p[12] + 2\ p[8] + p[4])). \end{aligned} \tag{A3}$$

The constant used in this equation reflects the differing sizes of grid cells at each latitude.

The direction of flow DIR is calculated as

$$\begin{aligned} \mathrm{DIR} = \arctan\left(\frac{w}{s}\right);\ & \text{added}180^\circ \text{ if } s \geq 0, \\ & \text{and } 360^\circ \text{ if } s < 0 \text{ and } w \geq 0. \end{aligned} \tag{A4}$$

The total shear vorticity VORT is the sum of the westerly and southerly vorticity.

$$\mathrm{VORT} = zw + zs, \tag{A5}$$

where zw corresponds to the difference of the westerly flow between 40°N and 50°N minus that between 50°N and 60°N.

$$\begin{aligned} zw = {} & 1.08\ (0.5\ (p[1] + p[2]) - 0.5\ (p[8] + p[9])) \\ & - 0.94\ (0.5\ (p[8] + p[9]) - 0.5\ (p[15] + p[16])). \end{aligned} \tag{A6}$$

And, zs is the difference of the southerly flow between 30°E and 20°E minus that between 10°E and 0°E.

$$\begin{aligned} zs = {} & 1.21\ (0.25\ (p[14] + 2\ p[10] + p[6]) \\ & - 0.25\ (p[13] + 2\ p[9] + p[5]) \\ & - 0.25\ (p[12] + 2\ p[8] + p[4]) \\ & + 0.25\ (p[11] + 2\ p[7] + p[3])). \end{aligned} \tag{A7}$$

References

Barry, R. G. and Carleton, A. M. 2001. *Synoptic and Dynamic Climatology*. Routledge, London, 620 pp.

Blenkinsop, S., Jones, P. D., Dorling, S. R. and Osborn, T. J. 2009. Observed and modelled influence of atmospheric circulation on central England temperature extremes. *Int. J. Climatol.* **29**, 1642–1660.

Christensen, J. H., Christensen, O. B., Lopez, P., van Meijgaard, E. and Botzet, M. 1996. The HIRHAM4 regional atmospheric climate

model. Scientific Report 96–4, The Danish Meteorological Institute, Copenhagen, Denmark.

Christensen, J. H., Boberg, F., Christensen, O. B. and Lucas-Picher, P. 2008. On the need for bias correction of regional climate change projections of temperature and precipitation. *Geophys. Res. Lett.* **35**, L20709, doi:10.1029/2008GL035694.

Coles, S. 2001. *An Introduction to Statistical Modeling of Extreme Values*. Springer Verlag, London, 208 pp.

Demuzere, M., Werner, M., van Lipzig, N. P. M. and Roeckner, E. 2009. An analysis of present and future ECHAM5 pressure fields using a classification of circulation patterns. *Int. J. Climatol.* **29**, 1796–1810.

Giorgi, F., Bi, X. and Pal, J. S. 2004. Mean, interannual variability and trends in a regional climate change experiment over Europe. I. Present-day climate (1961–1990). *Clim. Dyn.* **22**, 733–756.

Haylock, M. R., Hofstra, N., Klein Tank, A. M. G., Klok, E. J., Jones, P. D. and New, M. 2008. A European daily high-resolution gridded data set of surface temperature and precipitation for 1950–2006. *J. Geophys. Res.* **113**, D20119, doi:10.1029/2008JD010201.

Holtanová, E., Kalvová, J., Mikšovský, J., Pišoft, P. and Motl, M. 2010. Analysis of uncertainties in regional climate model outputs over the Czech Republic. *Stud. Geophys. Geod.* **54**, 513–528.

Hosking, J. R. M. 1990. L-moments: analysis and estimation of distributions using linear combinations of order statistics. *J. R. Statist. Soc. B* **52**, 105–124.

Isaaks, E. H. and Srivastava, R. M. 1989. *An Introduction to Applied Geostatistics*. Oxford University Press, New York, 561 pp.

Jacob, D. 2001. A note to the simulation of the annual and inter-annual variability of the water budget over the Baltic Sea drainage basin. *Meteorol. Atmos. Phys.* **77**, 61–73.

Jacob, D., Bärring, L., Christensen, O. B., Christensen, J. H., de Castro, M. and co-authors. 2007. An inter-comparison of regional climate models for Europe: model performance in present-day climate. *Clim. Change* **81**, 31–52.

Jenkinson, A. F. and Collison, F. P. 1977. An initial climatology of gales over the North Sea, Synoptic Climatology Branch Memorandum No. 62, Meteorological Office, Bracknell, U.K.

Kjellström, E., Bärring, L., Gollvik, S., Hansson, U., Jones, C. and co-authors. 2005. A 140-year simulation of European climate with the new version of the Rossby Centre regional atmospheric climate model (RCA3). *SMHI Reports Meteorology and Climatology* Volume 108, SMHI, SE-60176. Norrköping, Sweden, 54 pp.

Kjellström, E., Bärring, L., Jacob, D., Jones, R., Lenderink, G. and co-authors. 2007. Modelling daily temperature extremes: recent climate and future changes over Europe. *Clim. Change* **81**, 249–265.

Kjellström, E., Nikulin, G., Hansson, U., Strandberg, G. and Ullerstig, A. 2011. 21st century changes in the European climate: uncertainties derived from an ensemble of regional climate model simulations. *Tellus* **63A**, doi:10.1111/j.1600-0870.2010.00475.x

Kostopoulou, E., Tolika, K., Tegoulias, I., Giannakopoulos, C., Somot, S. and co-authors. 2009. Evaluation of a regional climate model using in situ temperature observations over the Balkan Peninsula. *Tellus* **61A**, 357–370.

Kyselý, J., Beranová, R., Picek, J. and Štěpánek, P. 2008. Simulation of summer temperature extremes over the Czech Republic in regional climate models. *Meteorologische Zeitschrift* **17**, 645–661.

Kyselý, J. 2010. Recent severe heat waves in central Europe: how to view them in a long-term prospect? *Int. J. Climatol.* **30**, 89–109.

Kyselý, J. and Plavcová, E. 2010. A critical remark on the applicability of E-OBS European gridded temperature data set for validating control climate simulations. *J. Geophys. Res.* **115**, D23118, doi:10.1029/2010JD014123.

Lenderink, G., van den Hurk, B., van Meijgaard, E., van Ulden, A. and Cujipers H. 2003. Simulation of present day climate in RACMO2: first results and model developments. KNMI, Technical Report 252, 24 pp.

Lenderink, G., van Ulden, A., van den Hurk, B. and van Meijgaard, E. 2007. Summertime inter-annual temperature variability in an ensemble of regional model simulations: analysis of the surface energy budget. *Clim. Change* **81**, 233–247.

Nikulin, G., Kjellström, E., Hansson, U., Strandberg, G. and Ullerstig, A. 2010. Evaluation and future projections of temperature, precipitation and wind extremes over Europe in an ensemble of regional climate simulations. *Tellus* **63A**, doi:10.1111/j.1600-0870.2010.00466.x.

Osborn, T. J., Conway, D., Hulme, M., Gregory, J. M. and Jones, P. D. 1999. Air flow influences on local climate: observed and simulated mean relationships for the United Kingdom. *Clim. Res*. **13**, 173–191.

Roeckner, E., Brokopf, R., Esch, M., Giorgetta, M., Hagemann, S. and co-authors. 2006. Sensitivity of simulated climate to horizontal and vertical resolution in the ECHAM5 atmosphere model. *J. Clim.* **19**, 3771–3791.

Samuelsson, P., Jones, C. G., Willén, U., Ullerstig, A., Gollvik, S. and co-authors. 2011. The Rossby Centre Regional Climate Model RCA3: Model description and performance. *Tellus* **63A**, this issue.

Sanchez-Gomez, E., Somot, S. and Déque, M. 2009. Ability of an ensemble of regional climate models to reproduce weather regimes over Europe-Atlantic during the period 1961–2000. *Clim. Dyn.* **33**, 723–736.

Seneviratne, S. I., Pal, J. S., Eltahir, E. A. B. and Schär, C. 2002. Summer dryness in a warmer climate: a process study with a regional climate model. *Clim. Dyn.* **20**, 69–85.

Štěpánek, P., Zahradníček, P. and Skalák, P. 2009. Data quality control and homogenization of air temperature and precipitation series in the area of the Czech Republic in the period 1961–2007. *Adv Sci. Res.* **3**, 23–26.

Turnpenny, J. R., Crossley, J. F., Hulme, M. and Osborn, T. J. 2002. Air flow influences on local climate: comparison of a regional climate model with observations over the United Kingdom. *Clim. Res.* **20**, 189–202.

Uppala, S. M., Kallberg, P. W., Simmons, A. J., Andrae, U. and co-authors. 2005. The ERA-40 re-analysis. *Q. J. R. Meteorol. Soc.* **131**, 2961–3012.

van der Linden, P. and Mitchell, J. F. B. (eds.) 2009. *ENSEMBLES: Climate Change and its Impacts: Summary of Research and Results from the ENSEMBLES Project*. Met Office Hadley Centre, Exeter, UK, 160 pp.

van Ulden, A., Lenderink, G., van den Hurk, B. and van Meijgaard, E. 2007. Circulation statistics and climate change in Central Europe: PRUDENCE simulations and observations. *Clim. Change* **81**, 179–192.